Chapter 2

Determination of MWD from G' and G''

2.1 INTRODUCTION

Over the last two decades, a number of publications (most notably [2-11]) has been devoted to the prediction of the molecular weight distribution, $w(M)$, of entangled linear polymers from their linear viscoelastic response. Although a considerable degree of success has been reached in the recent studies, more quantitative and robust predictions are yet to be obtained, specially for multimodal distributions. The variety of published models and techniques can be briefly described as follows.

First, on the theoretical side, two basic ingredients are used: (i) an analytical expression for the relaxation modulus, $G_{mono}(t, M)$, of the monodisperse system as a function of molecular weight, M, and (ii) a suitable mixing rule which relates the relaxation modulus of the polydisperse material, $G(t)$, to $w(M)$ and $G_{mono}(t, M)$. Ideally, the resulting mathematical model should have but few material parameters endowed with a clear physical or molecular interpretation. Over the years, various refinements of the classical de Gennes/Doi/Edwards reptation theory [12-13] have been used to model $G_{mono}(t, M)$, while mixing rules based on the Tsenoglou/des Cloizeaux concept of double reptation [14-16] have gained acceptance. Results reported recently in [19] and the companion paper [1] show that quantitative predictions are indeed obtained with such molecular models in the *direct* problem of computing

the relaxation modulus of entangled linear polymers from their known MWD.

Second, on the computational side, one must somehow deal with the ill-posed nature of the *inverse* problem of computing $w(M)$ from $G(t)$. Three basic approaches have been adopted in the literature. A regularization method is used in [5, 8, 9, 10], while stabilization is achieved in [4, 6] by computing the moments of the MWD. The third approach consists in assuming a parametric form for the MWD [7, 11]. A detailed comparison of the three approaches remains to be performed.

In the companion paper [1], we have evaluated the ability of three theoretical models, combined with double reptation, to solve the direct problem of computing $G(t)$ from $w(M)$: the basic Doi-Edwards theory, its extension to include tube length fluctuations [13], and the time-dependent diffusion (TDD) reptation model proposed by des Cloizeaux [20]. Theoretical predictions of the dynamic moduli (G', G'') computed using these models and the MWD data, measured by size exclusion chromatography (SEC), were systematically compared to experimental results for polystyrene (PS), high-density polyethylene (HDPE), and polycarbonate (PC) samples. Both monomodal (narrow or broad) and multimodal distributions were considered. We found that the TDD model, combined with double reptation (DR) and a suitable description of Rouse relaxation processes [1], is clearly superior and capable of quantitative predictions. For systems containing a significant fraction of short chains (slightly longer than the critical molecular weight), however, the TDD-DR model was found to predict too fast a relaxation. After a modification of the model, quantitative predictions were obtained for these systems as well [1]. We also found that the transition between reptation-dominated and Rouse-dominated regimes is correctly described by the proposed model for Rouse dynamics.

In the present paper, we address the inverse problem of computing $w(M)$ from $G(t)$ using the TDD-DR model, suitably modified to treat short chains and include Rouse processes. A parametric method is adopted to deal with the ill-posedness of the problem. The MWD is represented by a three-parameter generalized exponential (GEX) function, which is known to describe accurately a wide class of monomodal distributions [22]. In order to deal with multimodal systems, we also consider a seven-parameter double GEX (DGEX) description, obtained by com-

bining two GEX functions. For most of the PS, PC, and HDPE samples studied in [1], we compare the predicted and experimental molecular weight distributions. Agreement ranges from satisfactory to excellent. In particular, the DGEX methodology is able to resolve small amounts of short chains in bimodal blends with a high molecular weight component.

The paper is organized as follows. We display the modified TDD-DR model in Section 2, while Section 3 is devoted to the numerical approach. Section 4 gathers useful information on the studied materials. The results for monomodal (either narrow or broad) and bimodal samples are reported and discussed in Section 5. Finally, conclusions are drawn.

2.2 THEORY

The double reptation (DR) theory proposed by Tsenoglou [14, 15] and des Cloizeaux [16] relates the relaxation modulus $G(t)$ of an entangled linear polymer to its molecular weight distribution $w(M)$ through the mixing rule

$$G(t) = G_N^0 \cdot \left(\int_{\log M_e}^{\infty} [F_{mono}(t, M)]^{\frac{1}{\beta}} \cdot w(M) d\log(M) \right)^{\beta}. \qquad (2.1)$$

Here, G_N^0 is the plateau modulus, M_e is the molecular weight between entanglements, and $w(M) = dW(M)/d\log(M)$ with $W(M)$ being the weight fraction of chains with molecular weight below M. The original double reptation theory sets the mixing exponent β to a value of 2, but slightly higher values have been suggested which could represent contributions of higher-order entanglements involving more than two chains or could be linked to the tube dilation model [17, 18]. As in the companion paper [1], we consistently use $\beta = 2.25$. Finally, $F_{mono}(t, M)$ is the relaxation function of the monodisperse polymer of mass M. Inclusion of constraint release effects through double reptation yields

$$F_{mono}(t, M) = F_{sr}(t, M)^{\beta}, \qquad (2.2)$$

where $F_{sr}(t, M)$ is the simple reptation relaxation function in a fixed network of entanglements. In the present work, we adopt the time-dependent diffusion (TDD) reptation model proposed by des Cloizeaux [20]:

$$F_{sr}(t,M) = \frac{8}{\pi^2} \cdot \sum_{i\ odd} \frac{1}{i^2} \cdot \exp(-i^2 \cdot U(t,M)), \tag{2.3}$$

where $U(t,M)$ is given by

$$U(t,M) = \frac{t}{\tau_{rept}(M)} + \frac{M^\star}{M} \cdot g\left(\frac{M \cdot t}{M^\star \cdot \tau_{rept}(M)}\right). \tag{2.4}$$

Here, the function g is conveniently approximated [20] by

$$g(x) = -x + x^{0.5} \cdot \left[x + (\pi \cdot x)^{0.5} + \pi\right]^{0.5}. \tag{2.5}$$

In Eq.(2.4), the reptation time τ_{rept} is linked to the molecular weight through

$$\tau_{rept}(M) = K_{TDD} \cdot M^3. \tag{2.6}$$

In addition to G_N^0 and M_e (which are directly related), the TDD-DR model (2.1-2.6) has basically two material parameters, $M^\star$ and K_{TDD}.

We have shown in the companion paper [1] that the TDD-DR model provides truly quantitative predictions for high molecular weight polymers. For systems containing a significant fraction of short chains (namely $M < 4 \cdot M_e$), however, it does predict too fast a relaxation. A simple empirical modification of the model for short chains was found to provide excellent results [1]: while Eq. (2.2) remains valid for long chains ($M \geq 4 \cdot M_e$), one uses instead $F_{mono}(t,M) = F_{sr}(t,M)$ for short chains ($M < 4 \cdot M_e$), and rescales the reptation time τ_{rept} to τ_{rept}/β to ensure continuity.

Finally, as we shall see later, solution of the inverse problem requires in some cases to include Rouse relaxation processes in the analysis. For entangled polymers, relaxation processes at times much shorter than the reptation time are dominated by the Rouse mechanism. There is however a significant difference with respect to dilute solutions or unentangled polymer melts. After a time equal to τ_{Rouse}/N^2, where $N = M/M_e$ is the number of entanglements of the test chain, subchains with molar mass M_e are relaxed and the Rouse relaxation of longer subchains is hampered by the presence of the tube. Therefore, Rouse modes perpendicular to the tube cannot be activated for subchains longer than M_e. From this moment on the chain segments feel the constraint imposed by the

tube, and only longitudinal Rouse modes along the tube remain to be considered. Thus, the Rouse relaxation function of the monodisperse polymer is given by

$$F_{Rouse}(t,M) = \frac{1}{N} \cdot \left\{ \sum_{i=N}^{\infty} \exp(\frac{-i^2 \cdot t}{\tau_{Rouse}(M)}) + \frac{1}{3} \cdot \sum_{i=1}^{N} \exp(\frac{-i^2 \cdot t}{\tau_{Rouse}(M)}) \right\}. \tag{2.7}$$

The Rouse time τ_{Rouse} is linked to the molecular weight through

$$\tau_{Rouse}(M) = K_{Rouse} \cdot M^2, \tag{2.8}$$

where K_{Rouse} is a material parameter. The first term of Eq. (2.7) represents the Rouse relaxation process of the whole chain restricted to subchains smaller than M_e, and the second term considers the slower modes, but only in the longitudinal dimension (hence the factor 1/3). The basis of this expression comes from a formula proposed by Pattamaprom et al. [19]. Nevertheless, it differs by a factor $1/N$ in front of the exponentials. Indeed, Rouse relaxation of subchains shorter than the tube diameter must be identical to that of dilute polymer solutions or unentangled melts. This equivalence is guaranteed by Eq. (2.7) but not by the original formula by Pattamaprom et al. The modified equation also reflects the well known divergence of the Rouse modulus at vanishing times.

The Rouse contribution $G_{Rouse}(t)$ to the relaxation modulus is assumed to obey a linear mixing law,

$$G_{Rouse}(t) = G_N^0 \cdot \left(\int_{\log M_e}^{\infty} F_{Rouse}(t,M) \cdot w(M) d\log M \right), \tag{2.9}$$

and it is simply added to the reptation result of Eq. (2.1).

For later discussion, it is useful to illustrate the present model in the monodisperse case. Within the scaling factor G_N^0, the relaxation function reduces then to the sum of the modified-TDD and Rouse relaxation functions, respectively $F_{mono}(t,M)$ and $F_{Rouse}(t,M)$. The corresponding dynamic moduli G' and G'' are shown as continuous curves in Fig. 2.1 for three different molecular weights and values of material parameters typical of polystyrene. (Note that the dashed curves have been obtained

by neglecting Rouse processes.) While the high frequency results (here, above 10^3 rad/s) essentially overlap, and thus are useless regarding the inverse problem, there is an intermediate range of frequencies where inclusion of Rouse relaxation in the model does indeed provide information on the molecular weight. As discussed in [1], it is particularly important to include Rouse processes in the analysis of small chains, for which the reptation process begins before the end of Rouse relaxation.

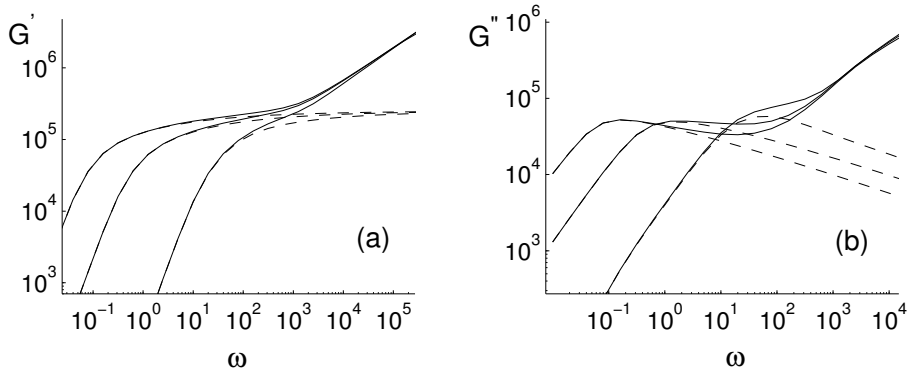

Figure 2.1: *Dynamic moduli predicted by the modified TDD model for monodisperse polystyrene, Rouse processes being either neglected (−−) or included (—). Results for* $M = 50000, 200000$ *and* 350000 *g/mol, using material data of Table 2.3.*

In summary, the TDD-DR model (2.1-2.8), suitably modified to treat short chains and include Rouse processes, provides a link between linear viscoelasticity and molecular weight distribution. The model involves only five material parameters, namely G_N^0, M_e, $M^\star$, K_{TDD}, and K_{Rouse}. In the companion paper [1], we have addressed the direct problem of predicting $G(t)$ (and thus the dynamic moduli G' and G'') from $w(M)$ data. The inverse problem is considered in the present paper.

2.3 NUMERICAL METHODOLOGY

2.3.1 GEX distribution functions

The inverse problem of determining MWD from dynamic moduli is known to be ill-posed. In order to alleviate this difficulty, Carrot and Guillet [7] and Nobile and co-workers [11, 21] restrict the space of feasible distributions to a 3-parameter family of generalized exponential (GEX) functions. Here, we follow this approach and extend it to take account of bimodal distributions.

The GEX distribution is a generalization of a large number of physically relevant molecular weight distributions, including those of Flory, Schultz, Tung and Weibull [22]. It is therefore an ideal parametric description of monomodal distributions, with more generality than the Gaussian or log-normal distributions. The GEX distribution is defined as

$$w_{GEX}(M) = C \cdot \left[\frac{M}{M_0}\right]^{a+1} \cdot \exp\left(-\left[\frac{M}{M_0}\right]^{b}\right), \tag{2.10}$$

and involves the three parameters a, b, and M_0. The normalization constant C is such that

$$\int w_{GEX}(M) d\log(M) = 1. \tag{2.11}$$

The corresponding weight-average and number-average molecular weights, respectively M_w and M_n, are given by

$$M_w = \int M \cdot w_{GEX}(M) d\log(M) = M_0 \cdot \Gamma\left(\frac{a+2}{b}\right) / \Gamma\left(\frac{a+1}{b}\right), \tag{2.12}$$

and

$$M_n^{-1} = \int M^{-1} \cdot w_{GEX}(M) d\log(M) = M_0^{-1} \cdot \Gamma\left(\frac{a}{b}\right) / \Gamma\left(\frac{a+1}{b}\right). \tag{2.13}$$

Large values of a and b yield a narrow distribution located near M_0. With the GEX representation, the inverse problem amounts to determine values of the three parameters a, b, and M_0 that provide

the best prediction of experimental dynamic moduli using the modified TDD-DR model.

We shall also consider bimodal systems, for which the following Double GEX (DGEX) description is useful:

$$w_{DGEX}(M) = p \cdot w_{GEX}^{(1)}(M) + (1-p) \cdot w_{GEX}^{(2)}(M). \tag{2.14}$$

where the proportion constant p is between 0 and 1, and each of the two GEX functions $w_{GEX}^{(i)}$ has parameters $a^{(i)}$, $b^{(i)}$, and $M_0^{(i)}$. The inverse problem thus amounts to determine optimal values for these seven parameters.

2.3.2 Error minimization

The input data is the set of experimental moduli $\{G'_{exp,i}, G''_{exp,i}\}$ measured at the frequency set $\{\omega_i\}$ for $i = 1, 2, \ldots, n_{exp}$. The corresponding set of theoretical moduli computed with the modified TDD-DR model for an assumed GEX or DGEX distribution is denoted by $\{G'_{theor,i}, G''_{theor,i}\}$.

We determine the optimal GEX or DGEX parameter values by a χ^2 minimization procedure, where the objective function is defined by

$$\chi^2 = \frac{1}{2 \cdot n_{exp}} \cdot \left(\sum_{i=1}^{n_{exp}} \frac{\left[G'_{exp,i} - G'_{theor,i}\right]^2}{\left[G'_{exp,i}\right]^2} + \sum_{i=1}^{n_{exp}} \frac{\left[G''_{exp,i} - G''_{theor,i}\right]^2}{\left[G''_{exp,i}\right]^2} \right). \tag{2.15}$$

A penalty term of order 10^{10} is added to χ^2 when the M_0 parameter (or one of the two $M_0^{(i)}$ parameters) would otherwise become negative during the course of the optimization process.

The optimal GEX or DGEX parameter values that minimize χ^2 are obtained by means of the Nelder-Mead simplex method [23], as implemented in the function `fmins` of MATLAB© 5.3. This is a direct search method which attempts to minimize a scalar-valued function of n real variables using only values of the function, but no information whatsoever on its derivatives (here, $n = 3$ or 7). At each iteration, the method updates a non-degenerate simplex in n-dimensional space, that is a geometric entity of non-vanishing volume which is the convex hull of $n + 1$

vertices (e.g. a triangle in 2-space, and a tetrahedron in 3-space). One or more test points are computed using simple geometric transformations (e.g. reflection and expansion) that often consist in moving the current vertex where the function value is largest. The function is evaluated at these candidate vertices, and a new simplex is generated such that its vertex values satisfy a suitable descent condition compared to the previous simplex. The iterations terminate when the simplex diameter is less than a specified tolerance. Alternatively, the termination criterion could require that the decrease in the function value be sufficiently small. To initialize the process, a single guess vertex is supplied from which an initial simplex is built. For a modern description and analysis of the Nelder-Mead algorithm, see [24].

Although the number of Nelder-Mead iterations is usually large, each iteration is parsimonious in function evaluations. This is important in the present context since the evaluation of χ^2 is expensive. For the latter, we proceed as follows. For given GEX or DGEX parameter values, the integrals of Eqs. (2.1) and (2.9) are discretized using a constant logarithmic increment in molecular weigth (typically, 25 discrete weights per decade). The theoretical moduli $G'_{theor,i}$ and $G''_{theor,i}$ are computed from the relaxation function $G(t)$ using the Schwarzl approximations [25]. For each frequency, this requires a total of 12 discrete evaluations of $G(t)$, and 2 linear combinations of those, with constant coefficients.

Suitable values of the GEX or DGEX parameters must be supplied to initialize the optimization process. While the initialization of the three GEX parameters is found to be rather inconsequential, the situation is more delicate with the seven DGEX parameters. We indeed observed that both the number of simplex iterations as well as the accuracy of the optimal DGEX MWD can be affected by inappropriate initial values. In order to solve both problems, we perform a preliminary optimization phase in two steps. First, the two GEX functions $w^{(i)}_{GEX}(M)$ are chosen very narrow (we set $a^{(1)} = b^{(1)} = a^{(2)} = b^{(2)} = 20$), and various values of the remaining three parameters $M_0^{(i)}$ and p are tested (typically 10 each); the combination that gives the smallest error χ^2 is retained as initial $M_0^{(i)}$ and p values for the simplex optimization. Second, with these frozen values for $M_0^{(i)}$ and p, different values (again, typically 10) for the remaining four parameters are tested with the constraint $a^{(1)} = b^{(1)} = a^{(2)} = b^{(2)}$, and the best combination provides the corresponding

initial values. The Nelder-Mead algorithm is thus ready to start. We consider that the iterations have converged when the absolute change in two successive χ-values is less than 10^{-4}.

2.4 EXPERIMENTAL RESULTS AND MATERIAL PARAMETERS

We consider various samples of three kinds of polymers exhibiting a wide range of dynamic behavior in the melt: polystyrene (PS), polycarbonate (PC), and high-density polyethylene (HDPE). Details on sample preparation, rheological measurement, and molecular characterization are given in the companion paper [1]. A summary is presented below.

2.4.1 Materials

PS: Narrow anionically polymerized samples have been obtained from various sources. Bidisperse samples have been prepared by solution blending from THF followed by precipitation with methanol and drying. Chemical stabilization has been ensured by addition of 3000 ppm antioxidant (Irganox 1076).
PC: Sample PC1 is a commercial linear bisphenol-A polycarbonate. Samples PC2 to PC4 are preparative size fractions of PC1. They have been obtained by Continuous Polymer Fractionation (CPF) following the procedure described in [26].
HDPE: PE1 is a broad industrial sample, prepared via multi-site Ziegler-Natta catalyst with density 0.958 and branching level below NMR spectroscopic detection limits. Samples PE2, PE3 and PE4 are narrow-disperse fractions obtained by Successive Solution Fractionation (SSF) of PE1 in cyclohexanone according to the procedure described in [27]. In order to avoid degradation during rheological measurement, the HDPE samples have been stabilized with Irganox B215 (3000 ppm).

2.4.2 Methods

SEC-UV measurements have been obtained for PC at room temperature in methylene chloride. Narrow PS standards (between 900000 and 1300 MW) and light scattering PC standards have been used for calibration

purposes. Absolute PC molecular weights have been obtained by universal calibration. Results of universal calibration have been checked against the available absolute PC standards and the agreement was within experimental error. Molar mass distributions of PS and HDPE have been measured with RI detection. Narrow PS standards covering the entire MW range of the samples have been used for calibration purposes. For PS, the mobile phase was THF and the temperature 40°C. For PE, SEC has been carried out at 135°C in 1,2,4-trichlorobenzene, stabilized with BHT (2 g/l). Universal calibration was used in both cases to obtain absolute molecular weights.

Dynamic storage and loss moduli have been determined on a strain-controlled rheometer (ARES from Rheometrics) in dynamic mode with a parallel-plate configuration at temperatures ranging from 140 to 200°C for PS, 160 to 220°C for PC and 140 to 220°C for PE. Linearity of the viscoelastic regime has always been checked beforehand with the help of a strain sweep. For PC, plates with a diameter of 8 mm have been used, in order to conserve the small available quantities of fractionated samples. For PS and PE, the usual 25 mm diameter plates have been used instead. The angular frequency sweep interval was 10^{-2} to 10^{2} rad/s, with a strain amplitude of 5% for PS and HDPE. The corresponding values for PC were 10^{-1} to 5.10^{2} for angular frequency and 15% for strain amplitude. All measurements have been performed under dry nitrogen atmosphere. Master curves (reference temperature of 170°C for PS, 200°C for PC and 190°C for PE) have been successfully calculated by applying the time-temperature superposition principle.

2.4.3 SEC results

Table 2.1 gives the SEC data for the various monomodal samples. Both narrow (PS) and broad (PC and HDPE) distributions are studied. We also consider PS samples having a bimodal distribution composed of two narrow peaks, obtained by blending two samples of Table 2.1. Their composition and SEC data are reported in Table 2.2. Consistency with the average molecular weights computed from the data of Table 2.1 is within 1% for all blends.

Table 2.1: *SEC molecular characterization of monomodal PS, PC, and HDPE samples [1]: average molecular weights M_w, M_n (g/mol), and polydispersity index $I_p = M_w/M_n$.*

PS	M_w	M_n	I_p	PC	M_w	M_n	I_p
PS1	355500	346200	1.03	PC1	22700	9600	2.36
PS2	191300	187600	1.02	PC2	11300	5700	1.98
PS3	886900	813500	1.09	PC3	23200	15300	1.52
PS6	58400	56900	1.03	PC4	39000	28000	1.39
PS8	676000	650900	1.04				

HDPE	M_w	M_n	I_p
PE1	145700	29700	4.91
PE2	87000	51700	1.68
PE3	121200	62600	1.94
PE4	136000	70000	1.94

2.4.4 Material parameters and frequency windows

We list in Table 2.3 the values of the modified TDD-DR material parameters for PS, PC, and HDPE. These have been obtained by solving the direct problem for *one* sample of each polymer (e.g. PC1 for PC). The parameter values which give the best fit for the chosen sample are used to solve either the direct problem [1] or the inverse problem (this work) for *any* other sample of the same polymer. In all cases tested, we found the results independent of the particular sample selected for the fit. Note that K_{Rouse} is not available for HDPE, as dynamic data could not be obtained at sufficiently high frequencies.

Finally, we report in Table 2.4 the experimental frequency window $[\omega_{min}^{exp}, \omega_{max}^{exp}]$ for which rheological data are available, as well as the observed cross-over frequency ω_{co}^{exp}. We also give the frequency window $[\omega_{min}^{th}, \omega_{max}^{th}]$ used for the inverse theoretical predictions (unless defined otherwise later in the text).

Table 2.2: *Composition and SEC molecular characterization of bimodal PS samples [1].*

Sample	Composition	M_w	M_n	I_p
PS9	(50% PS2, 50% PS3)	538600	308100	1.75
PS12	(65% PS2, 35% PS8)	361100	250200	1.44
PS14	(80% PS2, 20% PS6)	165000	128800	1.28

Table 2.3: *Modified TDD-DR material parameters used for both the direct [1] and inverse (this work) problems.*

Polymer Polymer	M_e (g/mol)	G_N^0 (Pa)	K_{TDD} (s.(mol/g)^3)	$M^\star$ (g/mol)	K_{Rouse} (s.(mol/g)^2)
PS	18500	2. 10^5	1.05 10^{-15}	160000	2. 10^{-12}
PC	2500	1.2 10^6	3.2 10^{-14}	50000	2. 10^{-12}
HDPE	1500	2.6 10^6	1.4 10^{-17}	70000	n.a.

2.5 RESULTS FOR MONOMODAL SAMPLES

2.5.1 Polystyrene

First, we consider results for PS1, which are illustrative of those obtained for the other narrow dispersed samples.

Inspection of Fig. 2.2a shows that the predicted MWD is in excellent agreement with the SEC data. The evolution of the predicted MWD during the course of the Nelder-Mead optimization procedure is illustrated in Fig. 2.2b. The initial vector of GEX parameters (a, b, M_0) is set to $(2, 2, 10^5)$, resulting in the dashed line distribution. As the iterations proceed, the predicted MWD first finds its location, and later adjusts its shape. Fig. 2.2c shows the evolution of the relative error χ on the dynamic moduli. While its initial value is about 100%, the error converges to 2% after about 300 iterations. The evolution of the predicted average molecular weights M_w and M_n is illustrated in Fig. 2.2d. Starting from the initial values $M_w = 112800$ and $M_n = 88600$ g/mol, they converge to $M_w = 353700$ and $M_n = 345100$, which is within the SEC data by 0.3% (Table 2.1).

We now consider results obtained under the same conditions, but for three different initial vectors (a, b, M_0) of GEX parameters (Fig. 2.3). Although the initial distributions are (on purpose) quite dissimilar, the

Table 2.4: *Frequency windows and cross-over frequency (rad/s).*

Sample	ω_{min}^{exp}	ω_{min}^{th}	ω_{co}^{exp}	ω_{max}^{th}	ω_{max}^{exp}
PS1	$7.2\ 10^{-3}$	$1.0\ 10^{-2}$	$1.6\ 10^{-1}$	$1\ 10^{0}$	$7.2\ 10^{3}$
PS9	$1.0\ 10^{-3}$	$1.0\ 10^{-3}$	$7.1\ 10^{-3}$	$5.0\ 10^{0}$	$1.0\ 10^{2}$
PS12	$7.2\ 10^{-4}$	$2.0\ 10^{-3}$	$4.0\ 10^{-1}$	$8.4\ 10^{2}$	$2.1\ 10^{3}$
PS14	$2.5\ 10^{-2}$	$4.0\ 10^{-2}$	$2.5\ 10^{0}$	$4.5\ 10^{3}$	$6.3\ 10^{3}$
PC1	$1.0\ 10^{-3}$	$1.6\ 10^{-1}$	$4.0\ 10^{1}$	$2.5\ 10^{3}$	$2.5\ 10^{5}$
PC2	$1.0\ 10^{0}$	$4.0\ 10^{0}$	$3.3\ 10^{2}$	$2.1\ 10^{3}$	$3.3\ 10^{4}$
PC3	$1.0\ 10^{-1}$	$1.6\ 10^{-1}$	$4.5\ 10^{1}$	$2.0\ 10^{3}$	$3.2\ 10^{5}$
PC4	$1.5\ 10^{-2}$	$2.3\ 10^{-2}$	$4.2\ 10^{0}$	$6.6\ 10^{2}$	$1.0\ 10^{4}$
PE1	$4.3\ 10^{-3}$	$2.5\ 10^{-2}$	$1.0\ 10^{2}$	$1.0\ 10^{2}$	$1.0\ 10^{2}$
PE2	$9.7\ 10^{-2}$	$1.5\ 10^{0}$	n.a.	$1.8\ 10^{2}$	$1.8\ 10^{2}$
PE3	$2.5\ 10^{-2}$	$4.0\ 10^{-2}$	$\sim 2.7\ 10^{2}$	$2.6\ 10^{2}$	$2.6\ 10^{2}$
PE4	$2.6\ 10^{-2}$	$4.1\ 10^{-2}$	$2.5\ 10^{2}$	$2.5\ 10^{2}$	$2.5\ 10^{2}$

iterative process does converge to basically identical results. The same conclusion holds for the optimal GEX parameters and predicted average weights (Table 2.5). The impact of the initialization is thus minimal, not only for PS1, but also for all monomodal samples of Table 2.1.

Table 2.5: *Monomodal PS1 sample : optimal GEX parameters and predicted average molecular weights and polydispersity index for various initial vectors (IV's) of GEX parameters.*

Initial vector	a	b	M_0	M_w	M_n	I_p
IV1 $= (2, 2, 10^5)$	11.245	3.922	272960	353700	345100	1.02
IV2 $= (1, 1, 10^6)$	10.727	4.037	280640	353700	344900	1.03
IV3 $= (10, 10, 10^5)$	11.199	3.799	268300	353700	344800	1.03
			SEC data:	355500	346200	1.03

The above results have been obtained using dynamic data $\{G'_{exp,i}, G''_{exp,i}\}$ measured in the frequency window $(\omega_{min}, \omega_{max}) = (10^{-2}, 10^{0})$ rad/s. Since Rouse processes fall outside this range (Fig. 2.4a), the Rouse contribution G_{Rouse} is discarded in the computations. We have again computed results under identical conditions, but for larger values of ω_{max}. They are given in Fig. 2.4b for various values of ω_{max} up to 10^1, and in Fig. 2.4c for $\omega_{max} = 10^2$. The corresponding optimal GEX parameters and predicted average molecular weights are listed in Table 2.6. In all cases, the initial vector of GEX parameters is set to $(2, 2, 10^5)$.

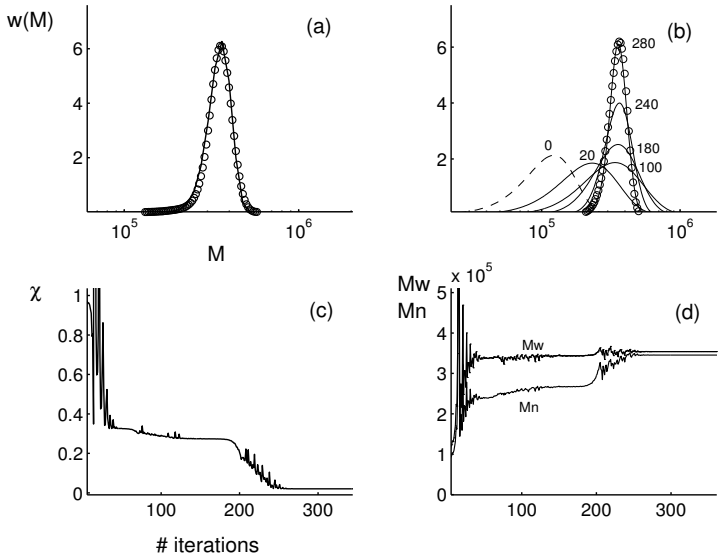

Figure 2.2: *Monomodal PS1 sample: (a) predicted distribution (—) and SEC data (∘); evolution of distribution (b), relative error on dynamic moduli (c), and average molecular weights (d) during the course of Nelder-Mead iterations.*

First, one observes that the average weights remain in good agreement with the SEC data, even though the Rouse processes have been neglected in the analysis. Second, the predicted MWD is only slightly affected by the choice of ω_{max} up to 10^1, but this is not the case for the optimal GEX parameters. Third, for $\omega_{max} = 10^2$, it is clearly wrong to ignore Rouse relaxation in the model, and the computed MWD clearly overpredicts the distribution of small weights.

The result of a similar computation, but now *including* the Rouse contribution G_{Rouse}, is shown in Fig. 2.4d for $\omega_{max} = 10^3$. Agreement with the SEC data is excellent. The predicted average weights are $M_w = 353500$ and $M_n = 343900$, and the corresponding optimal GEX parameters are $a = 11.349, b = 3.366, M_0 = 247300$. Clearly, inclusion of Rouse processes in the computations avoids the difficulty of selecting a suitable value for ω_{max}. The drawback, however, is that the computation time is essentially doubled.

Finally, we have also solved the inverse problem for PS1 using the

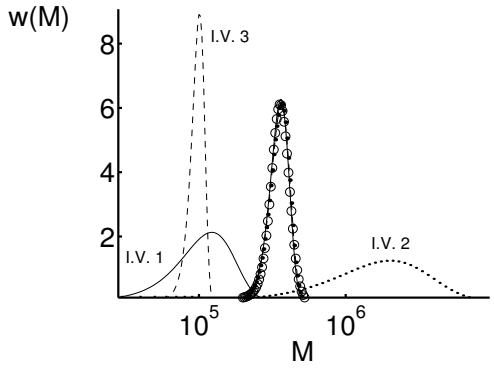

Figure 2.3: *Monomodal PS1 sample: initial and converged distributions for three different initial vectors (IV's) of GEX parameters (Table 2.5). The converged distributions do overlap with the SEC data (∘).*

Table 2.6: *Monomodal PS1 sample: optimal GEX parameters and predicted average molecular weights and polydispersity index for various values of* ω_{max} *(Rouse processes are* not *included in the analysis).*

ω_{max}	a	b	M_0	M_w	M_n	I_p
10^{-1}	18.682	2.215	133830	353900	345400	1.02
10^{0}	11.245	3.922	272960	353700	345100	1.02
$4.\,10^{0}$	17.930	2.192	134140	353600	344600	1.03
10^{1}	11.032	3.105	235030	353400	342800	1.03
10^{2}	2.833	82.617	439270	346300	322700	1.07
			SEC data:	355500	346200	1.03

DGEX distribution (2.14) intended for bimodal systems. Here, the frequency window is $(\omega_{min}, \omega_{max}) = (10^{-2}, 10^{0})$, and Rouse processes are thus neglected. We set the initial DGEX parameters $(a^{(i)}, b^{(i)}, M_0^{(i)})$ to $(2, 2, 10^5)$ and $(2, 2, 7.\,10^5)$, with a proportion factor $p = 0.5$. The initial distribution is shown in Fig. 2.5a together with the SEC data. The optimization process then evolves in three distinct phases. First, as shown in Fig. 2.5b, the two individual GEX functions converge to the same location forming together a single peak (e.g. the solid curve in Fig. 2.5c, which is made of the two GEX functions shown as dotted curves). In the second phase, the iterations keep the total distribution somewhat unaffected, but the proportion between the two GEX functions varies

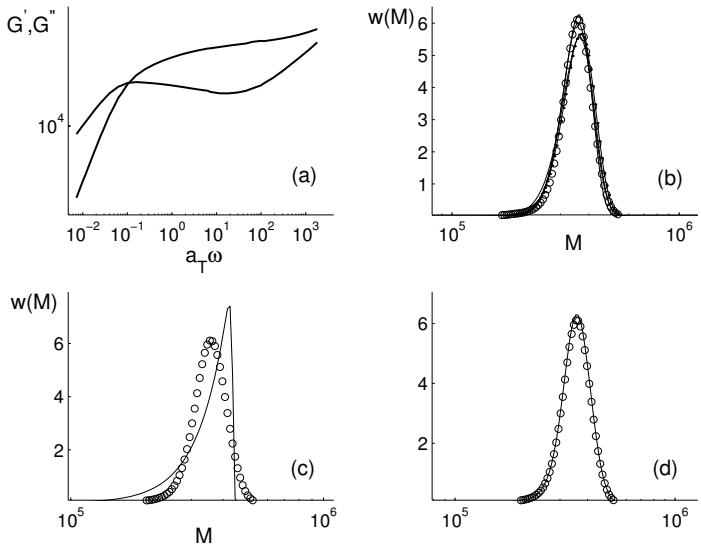

Figure 2.4: *Monomodal PS1 sample: (a) dynamic moduli [1]; predicted distribution (—) and SEC data (○): (b) Rouse processes neglected and* $\omega_{max} = 10^{-1}, 10^0, 4.10^0, 10^1$ *(results almost overlap), (c) Rouse processes neglected and* $\omega_{max} = 10^2$*, (d) Rouse processes included and* $\omega_{max} = 10^3$*.*

significantly so that one of them does not contribute any longer to the DGEX distribution (i.e. p has converged to either 0 or 1). Then, during the third phase shown in Fig. 2.5d, what has now become a monomodal GEX distribution converges to a final MWD which is very close indeed to the SEC data. Thus, solving the inverse problem for a monomodal system using the DGEX distribution indeed yields a monomodal MWD.

2.5.2 Polycarbonate

We now consider results obtained for the industrial PC1 sample, and three of its fractions, PC2, PC3 and PC4 (Fig. 2.6). Overall agreement with the SEC data is good. The frequency window for each case is such that Rouse processes can be ignored in the analysis. We found indeed that consideration of the Rouse relaxation and the complete experimental frequency range did not significantly improve the predicted MWD.

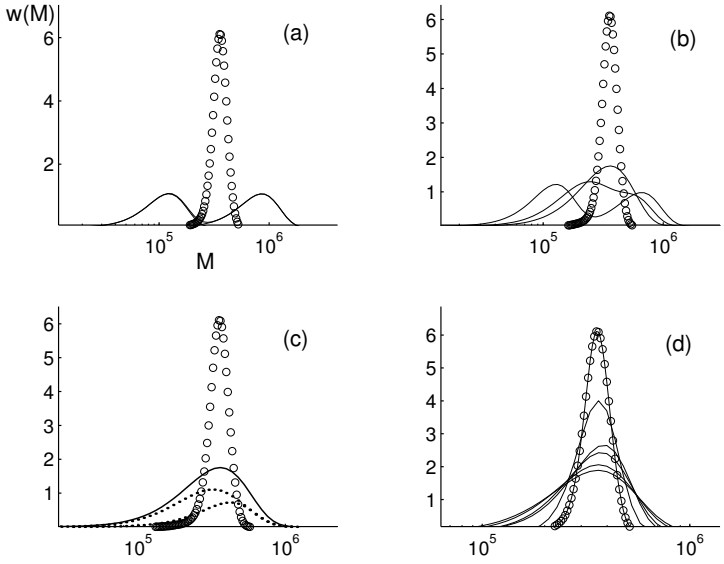

Figure 2.5: *Monomodal PS1 sample: evolution of DGEX distribution (—) during the course of Nelder-Mead iterations and SEC data (∘); (a) initial guess, (b) first phase of iterative process, (c) a particular iterate (—) made of two GEX functions (· · ·), (d) final phase of iterative process showing convergence to the SEC data.*

Table 2.7 gives the predicted average molecular weights. Their relative difference with the SEC data is of order 10%. We also list the final error χ on the dynamic moduli. It is a little higher than for the narrow disperse PS1 sample considered in the previous section. This is due to the somewhat noisier character of the dynamic data, specially for the smallest fraction PC2 [1]. Note that the error χ in the *direct* computation of dynamic moduli for PC2, using the modified TDD-DR model and the SEC data, is 27%, which is *larger* than the 18% for the inverse prediction.

The PC2 sample is typical of systems containing a significant fraction of short chains (namely $M < 4 \cdot M_e$). As explained in Section 2, we found it necessary when dealing with the direct problem [1] to modify the TDD-DR model for short chains. All results given in the present paper have been obtained with the modified TDD-DR model. It is instructive,

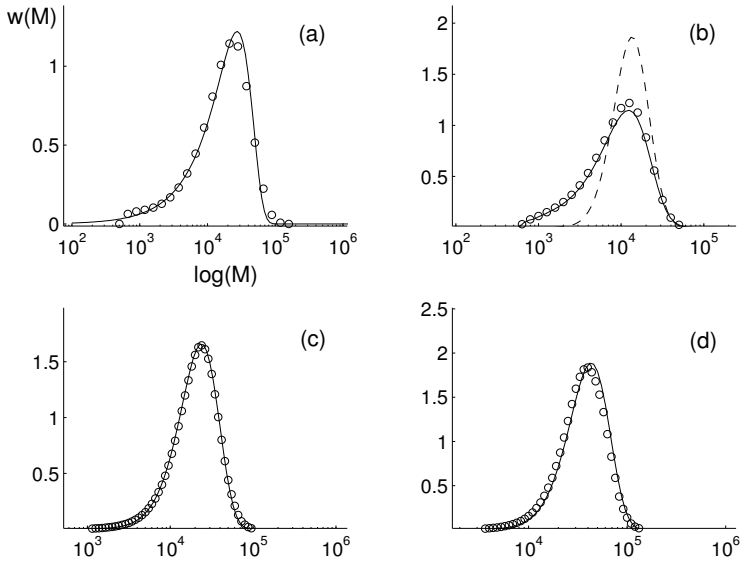

Figure 2.6: *Monomodal PC samples: predicted distribution (—) and SEC data (∘) for PC1 (a), PC2 (b), PC3 (c), and PC4 (d). The dashed curve in (b) has been obtained using the original TDD-DR model.*

however, to illustrate the importance of the proposed modification. To this end, we show in Fig. 2.6b the distribution obtained for PC2 using either the original (dashed curve) or modified (solid curve) TDD-DR model. The original model yields very poor results indeed, while the modified model is clearly superior.

2.5.3 Polyethylene

Obtaining an accurate MWD from rheological data for HDPE is more difficult than for PS or PC. This is partly due to the narrower dynamic range that is experimentally accessible. The maximum feasible frequency is of order 150 rad/s (Fig. 9 in [1]), which means that information regarding the relaxation of HDPE chains smaller than about 70000 g/mol is not available. Another reason is that, as we shall see, use of a single GEX function is not sufficient.

First, we discuss the illustrative results obtained for PE3. As shown in Fig. 2.7a, the predicted MWD is both correctly located and accurate

Table 2.7: *Monomodal PC samples: predicted average molecular weights and polydispersity index, and relative error on dynamic moduli.*

Sample	M_w	M_n	I_p	χ	M_w SEC	M_n SEC	I_p SEC
PC1	21000	8500	2.47	7%	22700	9600	2.36
PC2	12500	5300	2.36	18%	11300	5700	1.98
PC3	23000	15900	1.45	10%	23200	15300	1.52
PC4	41600	31700	1.31	7%	39000	28000	1.39

Table 2.8: *Monomodal PE3 sample: average molecular weights and polydispersity index, and relative error on dynamic moduli.*

Method	M_w	M_n	I_p	χ
SEC data	121200	62600	1.94	17%
GEX inverse problem	110700	38300	2.89	22%
GEX fit of SEC data	113200	64600	1.75	55%
DGEX fit of SEC data	124700	70400	1.77	42%
DGEX inverse problem	120600	60000	2.01	13%

for large molecular weights, but, as expected, it is not satisfactory for small weights. Thus, the predicted weight average M_w is within the SEC data by only 9%, while the number average M_n is off by 39 % (Table 2.8). The error χ on the dynamic moduli is 22%, which is slightly higher than that obtained in the direct problem using the SEC data (17%). This can be explained by the fact that a single GEX function is not enough in this case.

Indeed, it is useful to compute the best fit of the SEC data using a single GEX function. Contrary to the inverse problem, this operation, we insist, is but a purely mathematical exercise which does *not* involve any rheological model whatsoever. Inspection of Fig. 2.7b shows that this single-GEX fit is not very good for high molecular weights. As a result, it carries a large error (55%) in the direct prediction of dynamic moduli, much larger indeed that the single-GEX inverse prediction. Similarly, Fig. 2.7c shows the best DGEX mathematical fit of the SEC data, together with the two corresponding GEX functions. Although more accurate than the single-GEX fit, it is still not very good for high weights, and thus the error (again, of this direct problem) on the dynamic moduli remains large (42%) compared to that for the SEC data (17%). Finally,

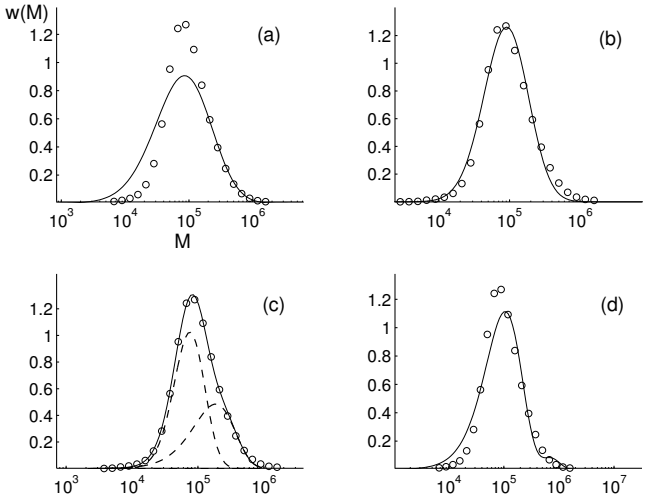

Figure 2.7: *Monomodal PE3 sample: computed distribution (—) and SEC data (∘); (a) GEX inverse prediction, (b) GEX best fit of SEC data, (c) DGEX best fit of SEC data (made of two GEX functions shown as dashed curves), (d) DGEX inverse prediction.*

the DGEX inverse prediction is reported in Fig. 2.7d. Note that the converged distribution still contains two distinct peaks (contrary to the case of the narrow PS1 sample). The presence of the small peak at large molecular weights yields an error on dynamic moduli (13%) that is smaller than that for the SEC data. The above results are gathered in Table 2.8.

Similar observations are made for the other HDPE samples. The GEX and DGEX inverse predictions are shown respectively in Fig. 2.8 and Fig. 2.9. The corresponding average molecular weights and error on dynamic moduli are given in Table 2.9. Overall, the quality of the DGEX inverse predictions is satisfactory.

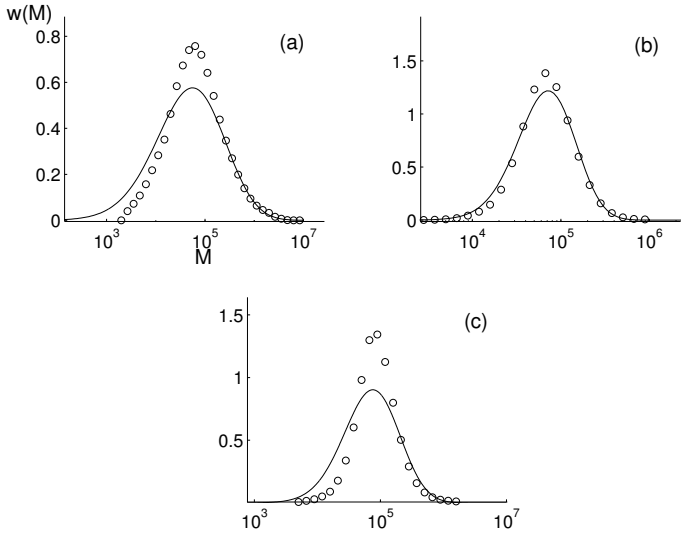

Figure 2.8: *Monomodal HDPE samples: GEX inverse prediction (—) and SEC data (∘) for PE1 (a), PE2 (b), and PE4 (c).*

2.6 RESULTS FOR BIMODAL SAMPLES

We now turn to the bimodal systems obtained by blending two narrow dispersed PS samples (Table 2.2). Unless stated otherwise, a DGEX distribution is used and the frequency window is such that Rouse processes can be neglected in the analysis.

The DGEX results for PS9 (made of 50% PS2 and 50% PS3) are shown in Fig. 2.10a. The predicted MWD is in quite good agreement with the SEC data. The evolution of the error χ on dynamic moduli during the optimization process is illustrated in Fig. 2.10b. In view of the preliminary optimization phase described earlier, the initial error is only 12%. After about 900 iterations, the error converges to 4%. Note that the SEC data gives an error of 8% in the direct problem. The evolution of the predicted average weights M_w and M_n is illustrated in Fig. 2.10c and d, for each of the two GEX functions $w_{GEX}^{(i)}$ making up the predicted MWD. The final values are listed in Table 2.10, and they agree very well with the SEC data. Note that the converged value of the p parameter in Eq.(2.14) yields 50.6% of PS2 in the blend, instead

Table 2.9: *Monomodal HDPE samples: predicted average molecular weights and polydispersity index, and relative error on dynamic moduli.*

Sample/Method	M_w	M_n	I_p	χ	M_w SEC	M_n SEC	I_p SEC
PE1/GEX	155800	24300	6.41	18%	145700	29700	4.91
PE1/DGEX	146000	26000	5.62	6%	145700	29700	4.91
PE2/GEX	84600	47000	1.80	11%	87000	51700	1.68
PE2/DGEX	90300	55300	1.63	4%	87000	51700	1.68
PE4/GEX	121500	42000	2.89	16%	136000	70000	1.94
PE4/DGEX	128400	51100	2.51	9%	136000	70000	1.94

of the actual 50%.

The inverse predictions for PS9 using only a single GEX function are shown in Fig 2.11a and Table 2.10. While the result for M_w is satisfactory, M_n is obviously way too small. The corresponding error on dynamic moduli is 20%. A GEX distribution is of course inappropriate for such bimodal systems.

Table 2.10: *Bimodal PS9 sample: predicted average molecular weights and polydispersity index.*

	M_w	M_n	I_p	M_w SEC	M_n SEC	I_p SEC
First DGEX peak	189000	185200	1.02	191300	187600	1.02
Second DGEX peak	900700	789000	1.14	886900	813500	1.09
DGEX for total sample	540600	297800	1.82	538600	308100	1.75
1 GEX for total sample	591700	179200	3.30	538600	308100	1.75

For completeness, we note that inclusion of Rouse processes and use of the full range of experimental frequencies (i.e. $\omega_{max} = 10^2$ rad/s instead of $5.\ 10^0$ in the above computations) do not alter the DGEX predictions for PS9 (Fig 2.11b).

Identical observations can be made with the DGEX predictions for the PS12 blend. As seen in Fig. 2.12 and Table 2.11, there is good agreement between the predictions and the SEC data. The converged value of the p parameter yields 58.7% of PS2 in the blend, instead of the actual 65%. The error χ is 2.8% for the DGEX inverse prediction, and 5.7% for the direct problem using the SEC data.

Finally, we assess the ability of the proposed DGEX methodology

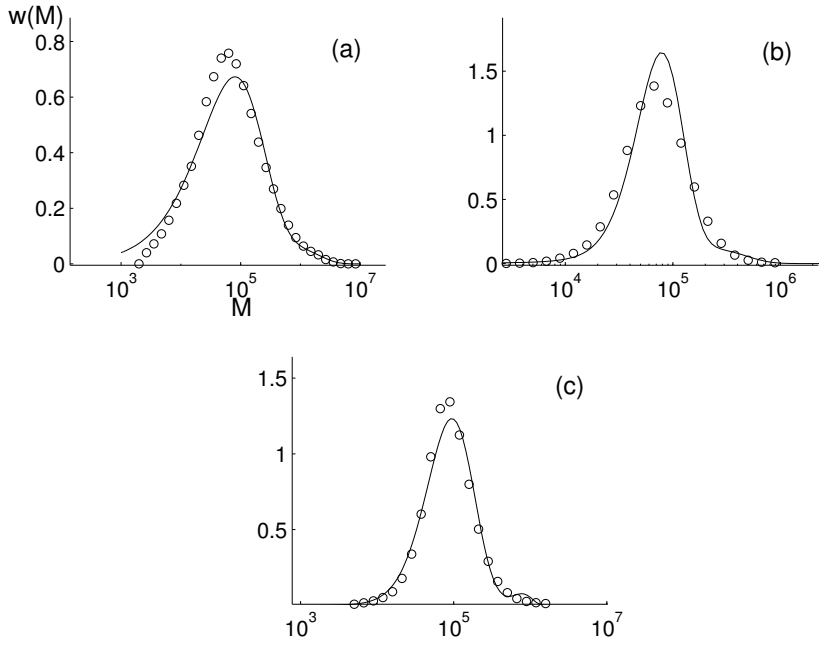

Figure 2.9: *Monomodal HDPE samples: DGEX inverse prediction (—) and SEC data (∘) for PE1 (a), PE2 (b), and PE4 (c).*

to resolve small amounts of a low-MW component blended with a high-MW sample. This is a very severe test indeed, where one would expect that consideration of the full range of available frequencies and inclusion of Rouse processes be quite beneficial. The results for PS14, which has 20% of short PS6 chains, are consistent with this expectation (see Fig. 2.13 and Table 2.12).

With reference to Fig. 2.13a, two computations have been made ignoring Rouse processes (respectively, with $\omega_{max} = 1$ and $7.\,10^1$), and one computation including Rouse processes (with $\omega_{max} = 4.\,10^3$). The first computation fails to resolve the short PS6 chains (Fig. 2.13b), although it does predict M_w rather well. The second computation, which neglects Rouse relaxation but considers a larger frequency range, yields much better results (Fig. 2.13c). It carries an error χ equal to 10%, and predicts 7.53% of short PS6 chains in the blend, instead of the actual 20%. The results including Rouse relaxation and the full range of avail-

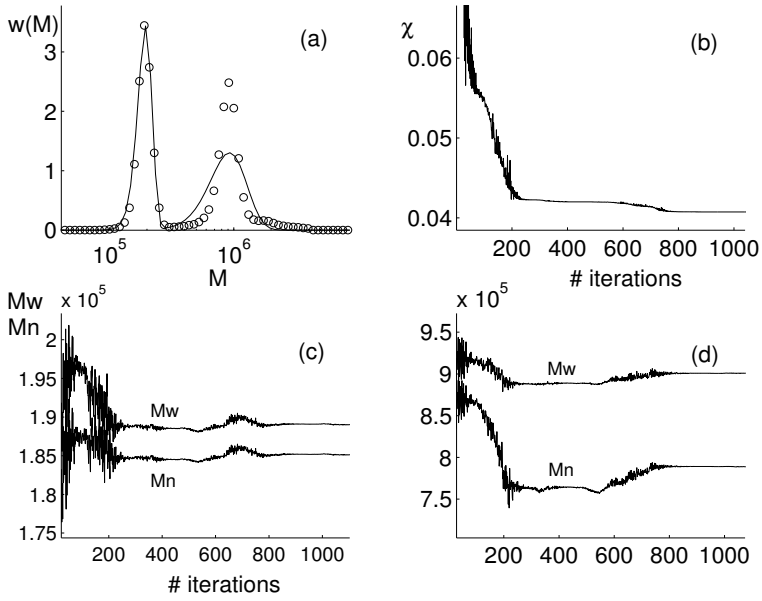

Figure 2.10: *Bimodal PS9 sample: (a) DGEX inverse prediction (—) and SEC data (○); evolution of relative error on dynamic moduli (b) and average molecular weights of the two peaks (c,d) during the course of Nelder-Mead iterations.*

able frequencies (Fig. 2.13d) clearly are superior. They predict 17.89% of short PS6 chains, and the error on dynamic moduli is down to 4%. The inverse predictions are in excellent agreement with the SEC data, and the methodology is indeed able to resolve the component of small molecular weight. The dynamic moduli computed using the predicted distribution are compared to the experimental data in Fig. 2.13a.

2.7 FREQUENCY WINDOW

As remarked by Carrot and Guillet [7], the accuracy of the molecular weight distribution prediction is mainly controlled by the lowest frequency that is experimentally accessible. They propose a criterion based on the crossover frequency ω_{co}^{exp}. For good accuracy (a few percent on M_w), the ratio $\omega_{min}^{exp}/\omega_{co}^{exp}$ between the minimum measured frequency

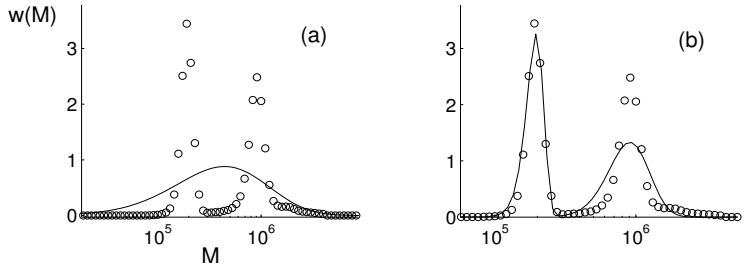

Figure 2.11: *Bimodal PS9 sample: inverse prediction (—) and SEC data (∘); (a) GEX distribution, (b) DGEX distribution and Rouse processes included.*

Table 2.11: *Bimodal PS12 sample: predicted average molecular weights and polydispersity index.*

	M_w	M_n	I_p	M_w SEC	M_n SEC	I_p SEC
First DGEX peak	175500	172000	1.02	191300	187600	1.02
Second DGEX peak	614100	550500	1.12	676000	650900	1.04
DGEX for total sample	356500	240100	1.48	361100	250200	1.44

and the crossover frequency has to be below 10^{-3}. This criterion seems applicable in our case for the HDPE samples, but not for the PS nor the PC samples (see Table 4). In the latter cases, excellent accuracy is obtained whereas $\omega_{min}^{exp}/\omega_{co}^{exp}$ is as high as 10^{-1} for narrow PS samples and of the order of 10^{-2} for PC samples. From our observations, it seems that the required $\omega_{min}^{exp}/\omega_{co}^{exp}$ ratio is a strongly decreasing function of polydispersity. This effet is clearly demonstrated by comparison between narrow PS1 and bimodal PS12 for instance (see Table 4). In the absence of a general criterion for the low frequency range, the safest strategy is to include a significant portion of the terminal zone in the experimental data.

One of the main conclusions of the present paper is the significance of the high frequency range for accurate determination of molecular weight distributions containing a sizable fraction of "short chains" (as defined by $M < 4M_e$). In this case, inclusion of the tube fluctuation-dominated frequencies is essential and so is the correct description of the TDD relaxation of the shortest chains by the proposed modified model. In the

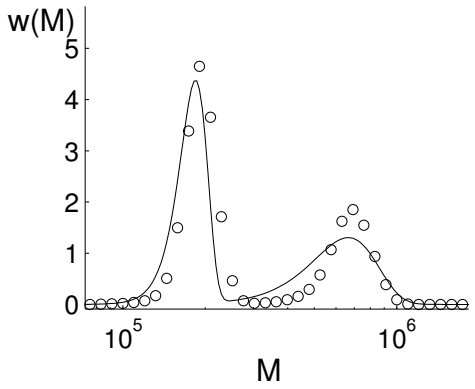

Figure 2.12: *Bimodal PS12 sample: DGEX inverse prediction (—) and SEC data (○).*

toughest cases, the transition to the Rouse-dominated frequencies has to be included as well. As the Rouse contribution to the dynamic moduli can be very roughly predicted even in the absence of prior knowledge of the molecular weight distribution, it is possible to assess if the experimentally accessible frequencies are high enough (see Table 4), provided that the parameters of the Rouse model are known. If the highest measured frequency is too low, accuracy in the low molecular weight range (and hence in the M_n-prediction) will predictably be less. It is important to keep in mind that accuracy of M_n determination by SEC is often poor because of the unfavourable number vs. weight ratio for short chains.

2.8 CONCLUSIONS

We have shown that the time-dependent diffusion, double reptation model of des Cloizeaux, suitably modified to treat short chains and include Rouse processes as suggested in the companion paper [1], can indeed be used with confidence to determine the molecular weight distribution of linear entangled polymers from their linear viscoelastic response. The results obtained for both monomodal (either narrow or broad) and bimodal systems are in quantitative agreement with size-exclusion chromatography data. In particular, the proposed inverse methodology is able to resolve small amounts of short chains in bimodal blends with a

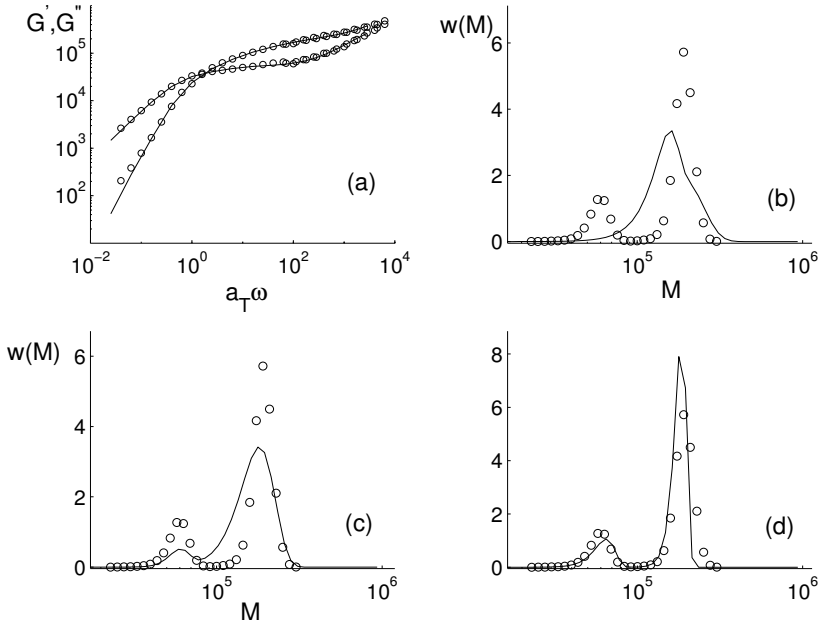

Figure 2.13: *Bimodal PS14 sample: (a) experimental (∘) dynamic moduli [1] and prediction (—) according to the DGEX result of (d); DGEX inverse prediction (—) and SEC data (∘): Rouse processes neglected and* $\omega_{max} = 1$ *(b) and* 7.10^1 *(c), Rouse processes included and* $\omega_{max} = 4.10^3$ *(d).*

high molecular weight component.

When confronted to an unknown sample, it is a priori difficult if not impossible to know whether the distribution is better represented by one or two GEX distributions, or whether the contributions from the Rouse modes can be neglected or not. It is therefore safest to take the complete experimental frequency range into consideration, include the Rouse contributions to the predicted relaxation modulus, and use the DGEX approach and the proposed initialization procedure.

Considering the level of quantitative accuracy achieved, is the inverse rheology method now a viable alternative or even a competitor of size exclusion chromatography? When assessing the respective merits of the two methods, it is important to consider issues of simplicity, sensitivity, and calibration.

Table 2.12: *Bimodal PS14 sample: predicted average molecular weights and polydispersity index,* ignoring *(#1: $\omega_{max} = 1$, #2: $\omega_{max} = 7.\,10^1$) or* including *($\omega_{max} = 4.\,10^3$) Rouse processes in the analysis.*

	M_w	M_n	I_p	M_w	M_n	I_p
	Rouse ignored #1			*Rouse ignored #2*		
First DGEX peak	141200	134700	1.05	58500	57100	1.02
Second DGEX peak	175800	154400	1.14	170100	157600	1.08
DGEX for total sample	164200	147200	1.12	161700	139200	1.16
	Rouse included			*SEC data*		
First DGEX peak	60100	58400	1.03	58400	56900	1.03
Second DGEX peak	178700	177400	1.01	191300	187600	1.02
DGEX for total sample	157500	130000	1.21	165000	128800	1.28

Ease of sample preparation and overall experimental simplicity and reproducibility clearly favour a rheology-based method, except in those few cases where material availability is an issue. Indeed, SEC is a very delicate procedure, especially when combined with on-line intrinsic viscosity (IV) or light scattering (LS) measurements, and requires highly specialized personnel to run reproducibly and reliably. This makes the inverse rheology prediction potentially more adapted for routine measurements.

Measurement sensitivity toward macromolecular species present at low concentration is quite different for the two techniques. Classical SEC detectors (UV or refractive index, RI) only see repeating units, independently of chain length. On-line coupling of SEC with IV and LS does increase sensitivity toward long chains (IV$\sim M^\alpha$ with $0.5 \leq \alpha \leq 0.8$; scattered light intensity $\sim M^2$). Unfortunately, interpretable LS and IV signals rarely cover the entire molecular weight distribution, which complicates the analysis. By contrast, viscoelastic measurements have a huge bias toward high molecular masses, considering the well known molecular weight dependence of the zero shear viscosity ($\eta_0 \sim M^\alpha$ with $\alpha > 3$). Very small amounts of high molecular weight chains become indeed detectable by rheology. This can lead to apparent discrepancies with SEC because such tiny concentrations might very well disappear in the background noise of UV or RI detectors. Some of our results for polyethylene point in this direction. It is important to keep in mind that the relaxation of long chains is affected by the presence of short ones,

in agreement with double reptation concepts as applied in this paper. Therefore, rheology is indeed sensitive to the presence of short chains. Further, inclusion of Rouse relaxation in the analysis improves the resolution of low molecular weight species, as we have shown. Overall, the sensitivity of the rheological method appears to be more balanced than could initially be expected. The excellent quantitative agreement observed for very different polymers and distributions confirms this analysis. In particular, the discrepancy between SEC results and inverse rheology predictions remains within the confidence interval of the SEC method itself (2 to 5 % standard relative error on M_w depending on the quality of the calibration). The method appears surprisingly accurate, even in situations where the frequency domain covered by the viscoelastic data does not span the range of relaxation times expected from the molecular distribution, as is the case for the HDPE samples studied. This is due in part to the self-consistency brought about by the use of GEX distributions. Also, rheology is very sensitive to polymer architecture (long chain branching), much more so than solution-based methods, and has at least the potential to reveal quantitative information about architecture. The inverse prediction of polymer architecture from linear viscoelasticity is still in its infancy but recent spectacular advances in the resolution of the direct problem [28, 29] suggest this goal may be within reach.

Calibration-related issues are very tricky for both SEC and rheology methods and deserve careful consideration. Before inverse predictions can be attempted, the parameters of the reptation and Rouse models require prior calibration. This is achieved (in principle once and for all) by fitting the experimental viscoelastic data for one sample in the direct problem, as shown in the companion paper [1]. Therefore, the molecular weight distribution of the calibration sample has to be known by independent means. Although knowledge of weight average molecular weight alone might be sufficient if a sample with very narrow distribution is available, which is rarely the case, the full distribution is required otherwise. Ideally, calibration samples for the inverse rheology prediction have to be independently characterized by SEC. As a consequence, the inverse rheology prediction cannot be considered totally independently from SEC, and is therefore not immune to SEC own set of thorny calibration issues. SEC and rheology are best viewed as complementary

methods, with the most information to be gained from critical comparisons and consistency checks between the two.

Bibliography

[1] E. van Ruymbeke, R. Keunings, V. Stéphenne, A. Hagenaars, C. Bailly, Evaluation of reptation models for predicting the linear viscoelastic properties of entangled linear polymers, Macromolecules 35 (2002) 2689-2699

[2] S. Wu, Polymer molecular weight distribution from dynamic viscoelastic properties, Polym. Eng. Sci. 25 (1985) 122-128

[3] W.H. Tuminello, Molecular weight and molecular weight distribution from dynamic measurements of polymer melts, Polym. Eng. Sci. 26 (1986) 1339-1347

[4] D.W. Mead, Determination of molecular weight distribution of linear flexible polymers from linear viscoelastic material functions, J. Rheol. 38 (1994) 1797-1827

[5] S.H. Wasserman, Calculating the molecular weight distribution from linear viscoelastic response of polymer melts, J. Rheol. 39 (1995) 601-625

[6] R.S. Anderssen, D.W. Mead, J.J. Driscoll, On the recovery of molecular weight functionals from the double reptation model, J. Non-Newtonian Fluid Mech. 68 (1997) 291-301

[7] C. Carrot, J. Guillet, From dynamic moduli to molecular weight distribution: A study of various polydisperse linear polymers, J. Rheol. 41 (1997) 1203-1220

[8] D. Maier, A. Eckstein, C. Friedrich, J. Honerkamp, Evaluation of models combining rheological data with the molecular weight distribution, J. Rheol. 42 (1998) 1153-1173

[9] F. Léonardi, A. Allal, G. Marin, Determination of the molecular weight distribution of linear polymers by inversion of a blending law on complex viscosities, Rheol. Acta 37 (1998) 199-213

[10] W. Thimm, C. Friedrich, M. Marth, J. Honerkamp, On the Rouse spectrum and the determination of the molecular weight distribution from rheological data, J. Rheol. 44 (2000) 429-438

[11] M.R. Nobile, F. Cocchini, Evaluation of molecular weight distribution from dynamic moduli, Rheol. Acta 40 (2001) 111-119

[12] P.-G. de Gennes, J. Chem. Phys., Reptation of a polymer chain in the presence of fixed obstacles, 55 (1971) 572-579

[13] M. Doi, S.F. Edwards, The Theory of Polymer Dynamics, Clarendon Press, Oxford, 1986

[14] C. Tsenoglou, Viscoelasticity of binary polymer blends, ACS Polym. Preprints 28 (1987) 185-186

[15] C. Tsenoglou, Molecular weight polydispersity effects on the viscoelasticity of entangled linear polymers, Macromolecules 24 (1991) 1762-1767

[16] J. des Cloizeaux, Double reptation versus simple reptation in polymer melts, Europhys. Lett. 5 (1988) 437-442

[17] M. Rubinstein, E. Helfand, D.S. Pearson, Theory of polydispersity effects on polymer rheology. Binary distribution of molecular weights, Macromolecules 20 (1987) 822-829

[18] G. Marrucci, Relaxation by reptation and tube enlargement: a model for polydisperse polymers, J. Polym. Sci. 23 (1985) 159-177

[19] C. Pattamaprom, R.G. Larson, T.J. Van Dyke, Quantitative predictions of linear viscoelastic rheological properties of entangled polymers, Rheol. Acta 39 (2000) 517-531

[20] J. des Cloizeaux, Relaxation and viscosity anomaly of melts made of entangled polymers. Time dependent reptation, Macromolecules 23 (1990) 4678-4687

[21] M.R. Nobile, F. Cocchini, J.V. Lawler, On the stability of molecular weight distributions as computed from the flow curves of polymer melts, J. Rheol. 40 (1996) 363-382

[22] J. Brandrup, E.H. Immergut (Eds.), Polymer Handbook, 4th. Ed., Wiley, New York, 1999

[23] J.A. Nelder, R. Mead, A simplex method for function minimization, Computer J. 7 (1965) 308-313

[24] J.C. Lagarias, J.A. Reeds, M.H. Wright, P.E. Wright, Convergence properties of the Nelder-Mead simplex algorithm in low dimensions, SIAM J. Optim. 9 (1998) 112-147

[25] F.R. Schwarzl, Numerical calculation of storage and loss modulus from stress relaxation data for linear viscoelastic materials, Rheol. Acta 10 (1971) 166-173

[26] A. Hagenaars, J.-J. Pesce, C. Bailly, B.A. Wolf, Characterization of melt-polymerized polycarbonate: preparative fractionation, branching distribution and simulation, Polymer 42 (2001) 7653-7661

[27] V. Stéphenne, C. Bailly, H. Berghmans, D. Daoust, P. Godard, Successive Solution Fractionation (SSF: a method to produce narrow dispersed polyethylenes), in preparation

[28] N.J. Inkson, T.C.B. McLeish, Predicting low density polyethylene melt rheology in elongational and shear flows with "pom-pom" constitutive equations, J. Rheol. 43 (1999) 873-896

[29] T.C.B. McLeish, S.T. Milner, Entangled dynamics and melt flow of branched polymers, Adv. Polym. Sci. 143 (1999) 195-256